2020 American Control Conference
Denver, CO, USA, July 1-3, 2020

Adaptive Quasi-Static Control of Multistable Systems

Adam L. Bruce, Nima Mohseni, Ankit Goel, and Dennis S. Bernstein

Abstract— **In some applications of control, the objective is to optimize the constant asymptotic response of the system by moving the state of the system from one forced equilibrium to another. Since suppression of the transient response is not the main objective, the feedback control law can operate quasi-statically, that is, extremely slowly relative to the open-loop dynamics. Although integral control can be used to achieve the desired setpoint, three issues must be addressed, namely, nonlinearity, uncertainty, and multistability, where multistability refers to the fact that multiple locally stable equilibria may exist for the same constant input. In fact, multistability is the mechanism underlying hysteresis. The present paper applies an adaptive digital PID controller to achieve quasi-static control of systems that are nonlinear, uncertain, and multistable. The approach is demonstrated on multistable systems involving unmodeled cubic and backlash nonlinearities.**

I. Introduction

Most applications of control, such as aircraft flight control and active noise and vibration suppression, require sensors and actuators with sufficient bandwidth, accuracy, and authority to significantly modify the dynamics of the plant, especially for stabilization. Unfortunately, even with ideal sensors and actuators, there are inherent limitations on the achievable closed-loop performance [1], [2].

In some applications, however, the ultimate objective is not to influence the dynamics of the plant, but rather to modify its asymptotic behavior. In these cases, stabilization is not feasible, nor are command following and disturbance rejection other than for step commands and step disturbances. In fact, applications of this type can be viewed as online optimization problems, where the control inputs may be parameters that can be adjusted to improve the performance of the system. Since the control algorithm operates at a much slower rate than the natural dynamics of the system, we refer to these applications as *quasi-static control problems.* A quasi-static controller thus makes no attempt to suppress the natural dynamics of the system, and certainly has no ability to stabilize the plant. Instead, the goal of an adaptive quasi-static controller is to slowly move the system from one forced equilibrium to another.

There are numerous applications of quasi-static control. For example, in flight control, it is necessary to move the aircraft trajectory from one trim state to another trim state, for example, cruise to descent. Another application is shape control of structures, such as a flexible membrane that serves as an optical reflector. Yet another application is the power grid, where voltages and power sources can be adjusted slowly to account for changing loads, and where fast transients are either ignored or left to separate, fast controllers. In these and other applications, the transient response is of secondary importance to the asymptotic steady-state behavior. From a control perspective, the goal is thus to determine a sequence of constant inputs that move the system to a desired forced equilibrium.

Since quasi-static control can follow only static commands and reject only constant disturbances, it is natural to apply integral control, where the integral action provides both command following and disturbance rejection. This approach requires consideration of three main issues, namely, nonlinearity, uncertainty, and multistability. First, adjustable plant parameters that serve as control "inputs" often appear nonaffinely in the plant dynamics, and thus the control problem may be highly nonlinear. Next, the structure of the forced equilibria may arise from static maps that are poorly known, thus making the plant uncertain. Finally, for a given constant control input, the system may have multiple asymptotically stable forced equilibria. A system of this type is called *multistable* [3]–[6].

Multistability is the key property of a hysteretic system, where the hysteresis loop arising from asymptotically low-frequency periodic forcing indicates that the state of the system is attracted to one set of equilibria as the input slowly increases, and to a different set of equilibria as the input slowly decreases [7]. In special cases, the hysteresis loop is identical to the shape of the asymptotic input-output phase portrait under periodic forcing; this phenomenon is called "rate-independent hysteresis." When this is not the case, the hysteresis is called "rate dependent." However, the nomenclature in both cases is misleading since hysteresis per se is a quasi-DC phenomenon [8], [9].

There are various models of systems that exhibit hysteresis, including Preisach, Duhem, Prandtl-Ishlinskii, Bouc-Wen, and Lur'e (nonlinear feedback) [10]–[15]. These models can be distinguished by various features, such as reversal behavior, the presence and properties of minor loops, and the set of forced equilibria. In particular, the set of forced equilibria may consist of isolated points or it may be a continuum.

As might be expected, multistability makes it difficult to approach quasi-static control as a problem of static function optimization. In particular, if the system were not multistable, then it would be feasible to probe the system with constant inputs and use the resulting asymptotic response to estimate gradients, which could be used subsequently to determine search directions for optimization. Multistability, however,

Adam L. Bruce, Nima Mohseni, Ankit Goel, and Dennis S. Bernstein are with the Department of Aerospace Engineering, University of Michigan, Ann Arbor, MI 48109, USA, admbruce@umich.edu, nmohseni@umich.edu, ankgoel@umich.edu, dsbaero@umich.edu.

precludes this possibility since the potential asymptotic responses corresponding to each constant input define a multivalued mapping, thus confounding the estimation of gradients.

Control of systems with hysteresis is addressed in [16] using inversion techniques; adaptive methods are used in the case where the hysteretic nonlinear is uncertain. A review of techniques used to control multistable systems is given in [17]. Neither [16] nor [17], however, considers the problem of quasi-static control.

The present paper focuses on quasi-static control of uncertain multistable systems. Since the goal is to follow commanded setpoints, integral control is used. In particular, since the plant dynamics may be uncertain, the present paper focuses on adaptive quasi-static PID control, which minimizes the reliance on analytical or empirical modeling and avoids manual tuning of the PID gains. In particular, the present paper applies the adaptive digital PID controller developed in [18]. To illustrate the approach, we consider multistable systems that have either isolated forced equilibria or a continuum of forced equilibria.

The next section reviews the adaptive digital PID control algorithm. In Section III, this algorithm is applied to quasi-static control of a system with a cubic nonlinearity as well as systems with a single or double backlash nonlinearity.

II. Adaptive Digital PID Control Algorithm

Consider the PID controller

$$v_k = K_{\mathrm{p},k} z_{k-1} + K_{\mathrm{i},k} \gamma_{k-1} + K_{\mathrm{d},k}(z_{k-1} - z_{k-2}), \quad (1)$$

where $K_{\mathrm{p},k}, K_{\mathrm{i},k}, K_{\mathrm{d},k}$ are time-varying gains to be adapted, z_k is the error variable, and, for all $k \geq 0$,

$$\gamma_k \triangleq \sum_{i=0}^{k} z_i. \quad (2)$$

Note that the integrator state can be computed recursively using $\gamma_k = \gamma_{k-1} + z_k$. Furthermore, the control (1) can be written as

$$v_k = \phi_k \theta_k, \quad (3)$$

where, for all $k \geq 0$,

$$\phi_k \triangleq [z_{k-1} \;\; \gamma_{k-1} \;\; z_{k-1} - z_{k-2}], \quad \theta_k \triangleq \begin{bmatrix} K_{\mathrm{p},k} \\ K_{\mathrm{i},k} \\ K_{\mathrm{d},k} \end{bmatrix}. \quad (4)$$

To determine the controller gains θ_k, let $\theta \in \mathbb{R}^3$, and consider the *retrospective performance variable* defined by

$$\hat{z}_k(\theta) \triangleq z_k + \sigma(\phi_{k-1}\theta - u_{k-1}), \quad (5)$$

where θ is obtained by optimization shown below, and σ is either 1 or -1 depending on whether the sign of the leading numerator coefficient of the transfer function from v_k to z_k is positive or negative, respectively. Furthermore, define the *retrospective cost function* $J_k \colon \mathbb{R}^3 \to [0, \infty)$ by

$$J_k(\theta) \triangleq \sum_{i=0}^{k} \hat{z}_k(\theta)^2 + (\theta - \theta_0)^{\mathrm{T}} P_0^{-1} (\theta - \theta_0), \quad (6)$$

where $\theta_0 \in \mathbb{R}^3$ is the initial vector of PID gains and $P_0 \in \mathbb{R}^{3\times 3}$ is positive definite. For all examples in this paper, we set $\theta_0 = 0$; however, θ_0 can be initialized to nonzero gains in practice if desired.

Proposition 2.1: Consider (3)–(6), where $\theta_0 \in \mathbb{R}^3$ and $P_0 \in \mathbb{R}^{3\times 3}$ is positive definite. Furthermore, for all $k \geq 0$, denote the minimizer (6) of J_k by

$$\theta_{k+1} \triangleq \operatorname*{argmin}_{\theta \in \mathbb{R}^n} J_k(\theta). \quad (7)$$

Then, for all $k \geq 0$, θ_{k+1} is given by

$$\theta_{k+1} = \theta_k + P_{k+1} \phi_{k-1}^{\mathrm{T}} [z_k + \sigma(\phi_{k-1}\theta_k - u_{k-1})], \quad (8)$$

where

$$P_{k+1} = P_k - \frac{P_k \phi_{k-1}^{\mathrm{T}} \phi_{k-1} P_k}{1 + \phi_{k-1} P_k \phi_{k-1}^{\mathrm{T}}}. \quad (9)$$

III. Adaptive Quasi-Static Control of Multistable Systems

This section investigates the performance of the adaptive digital PID controller applied to adaptive quasi-static control (AQC). Three illustrative examples are considered, namely, a cubic system, a single-backlash system, and a double-backlash system. The first example has isolated forced equilibria, whereas the remaining examples have a continuum of forced equilibria.

For each example, the sample time T_{s} of the digital controller is chosen to be significantly longer than the slowest time constant of the continuous-time system. In addition, the command for AQC is a step-dwell, where the length of time of each step is longer than T_{s}.

For all simulations of the sampled-data closed-loop systems, the fixed-step integration time is chosen to be 10^{-6} sec in order to capture the intersample response of the system.

A. AQC of the Cubic System

Consider the cubic system

$$\dot{q}(t) = q(t) - q^3(t) + u(t), \quad (10)$$

where $q(t)$ and $u(t)$ are scalar signals. For a constant input $u(t) \equiv \overline{u}$, the system has forced equilibria at the roots of $q - q^3 + \overline{u} = 0$. In particular, for all $\overline{u} < -0.42$ and $\overline{u} > 0.42$, (10) has one forced asymptotically stable equilibrium; for $\overline{u} = -0.42$ and $\overline{u} = 0.42$, (10) has two locally asymptotically forced equilibria; and, for all $\overline{u} \in (-0.42, 0.42)$, (10) has three forced equilibria, two of which are locally asymptotically stable and the third is unstable. Because of the existence of multiple asymptotically stable equilibria for a given value of $\overline{u}$, the system is multistable, and thus the forced equilibrium that q approaches depends on the input and the state history.

Let $q(0) = 0$ and let u be given by

$$u(t) = \begin{cases} -1.5 + 0.1 \left\lfloor \dfrac{t}{T_{\mathrm{d}}} \right\rfloor, & t \leq 30 T_{\mathrm{d}}, \\ 1.5 - 0.1 \left\lfloor \dfrac{t - 30T_{\mathrm{d}}}{T_{\mathrm{d}}} \right\rfloor, & t > 30 T_{\mathrm{d}}, \end{cases} \quad (11)$$

where $\lfloor x \rfloor$ is the largest integer smaller than x. Note that (11) is a sequence of steps, where each step is applied with dwell time $T_{\rm d} = 2$ sec. Figure 1 shows the equilibria achieved by (10) with the excitation (11). It can be seen that (10) has two asymptotically stable equilibria when the magnitude of $u(t)$ is between -0.42 and 0.42.

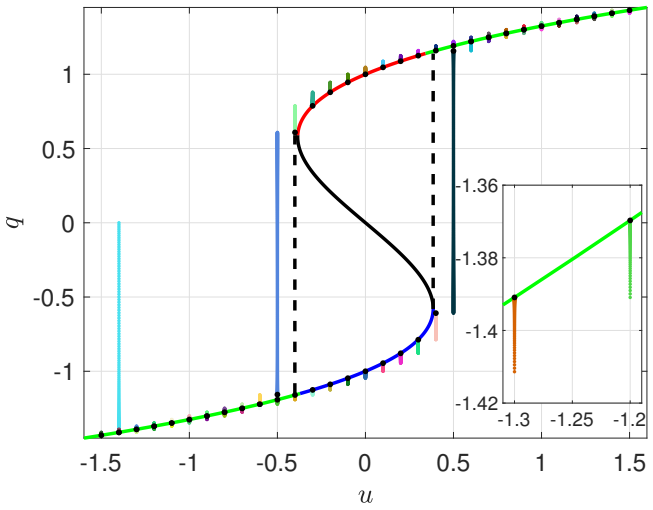

Fig. 1: Open-loop response of the cubic system (10) obtained with the step-dwell excitation $u(t)$ given by (11). The solid curve shows the forced equilibria of (10), which are the roots of $q - q^3 + u = 0$ for the corresponding constant value of u. Each point on the green curves corresponds to a unique asymptotically stable forced equilibrium. In addition, each point on the blue and red curves corresponds to a locally asymptotically stable forced equilibrium. The black curve indicates unstable equilibria of the system. The dashed vertical segments indicate jumps of the quasi-static system for either increasing or decreasing quasi-static inputs. The colored vertical line segments show the trajectory of q for each value of the step. Note that each trajectory converges to one of the forced equilibria. The large vertical line segment near -1.5 is due to the initial condition of the cubic system. The inset shows details of the transient response.

Figure 2 shows the zoomed-in open-loop response of (10) with the step-dwell excitation (11). Note that q converges for each step.

Next, consider adaptive quasi-static PI control of the cubic system (10). In this and the following examples, the derivative feedback gain $K_{\rm d}$ is set to zero. The step-dwell command $r(t)$ is given by

$$r(t) = \begin{cases} -1.5 + 0.3\left\lfloor \dfrac{t}{T_{\rm d}} \right\rfloor, & t \le 10T_{\rm d}, \\ 1.5 - 0.3\left\lfloor \dfrac{t - 10T_{\rm d}}{T_{\rm d}} \right\rfloor, & t > 10T_{\rm d}, \end{cases} \tag{12}$$

with dwell time $T_{\rm d} = 1000$ sec. The control $u(t)$ is updated with sample time $T_{\rm s} = 2$ sec, that is, for $t \in \{k, k + T_{\rm s}\}$,

$$u(t) = v_k, \tag{13}$$

where v_k is given by (1) and

$$z_k = r(kT_{\rm s}) - q(kT_{\rm s}). \tag{14}$$

Figure 3 shows the closed-loop response of the cubic system (10) under quasi-static control. Note that the adaptive quasi-static controller cannot stabilize the system but rather focuses on moving the state from one asymptotically stable equilibrium to another. Consequently, q does not converge in the case where, for all constant values of u, the commanded state of (10) is not an asymptotically stable equilibrium.

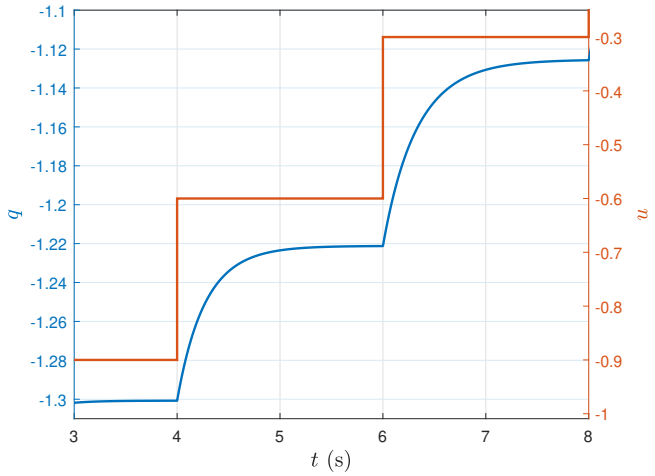

Fig. 2: Open-loop transient response of the cubic system (10) with step-dwell excitation. Each step is applied with dwell time $T_{\rm d} = 2$ sec, and the state q converges for each step.

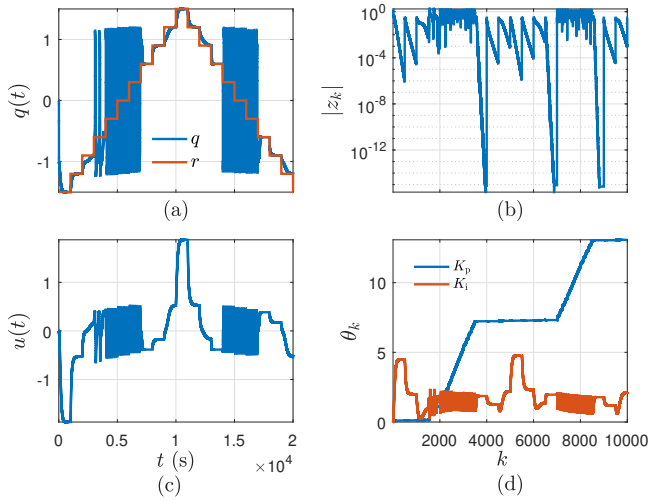

Fig. 3: Closed-loop response of the cubic system (10) with the step-dwell command (11) using adaptive quasi-static PI control. (a) shows the state $q(t)$, (b) shows the error variable z_k, (c) shows $u(t)$ given by the adaptive PI controller, and (d) shows the evolution of the gains $K_{{\rm p},k}$ and $K_{{\rm i},k}$.

Finally, Figure 4 shows the input-output phase portrait of closed-loop response of the cubic system (10) under quasi-static control. The converged values of q are shown in large colored dots.

B. AQC of the Single-Backlash System

The equation of motion for single-backlash system shown in Figure 5 is given by

$$m\ddot{q}(t) + c\dot{q}(t) + kd_{2w}(u(t) - q(t)) = 0, \tag{15}$$

where

$$d_{2w}(x) \triangleq \begin{cases} x - w, & x > w, \\ 0, & |x| \le w, \\ x + w, & x < -w. \end{cases} \tag{16}$$

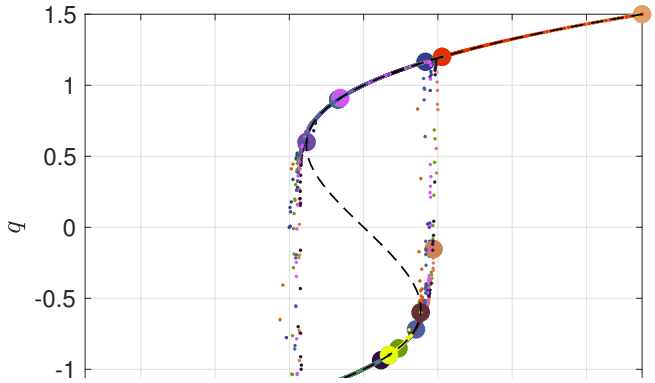

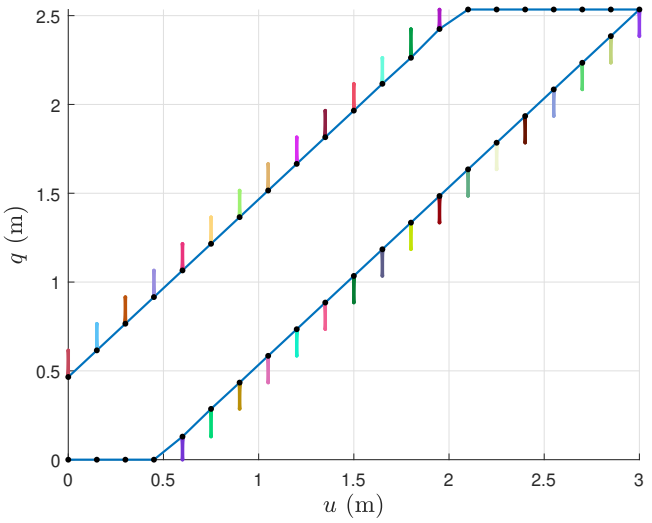

Fig. 6: Open-loop response of the single-backlash system (15) obtained with the step-dwell excitation (17). Each point on the blue curves corresponds to a Lyapunov- stable forced equilibrium and satisfies $d_{2w}(q-u)=0$. The colored vertical line segments show the trajectory of q for each step. The lower three points on the bottom left are due to the initial conditions of the single-backlash system.

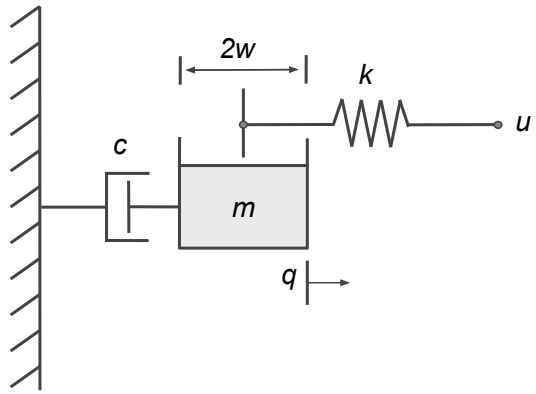

Fig. 5: Single-backlash system. The input u is the position of the right-hand endpoint of the spring, and the output q is the position of the right-hand edge of the mass. The width of the backlash is $2w$.

Let $m=1$ kg, $c=10$ N-s/m, and $k=100$ N/m, $w=0.5$ m, and $q(0)=\dot{q}(0)=0$, and let u be given by the step-dwell signal

$$u(t)=\begin{cases}0.15\left\lfloor\dfrac{t}{T_{\rm d}}\right\rfloor, & t\leq 20T_{\rm d},\\ 1.5-0.15\left\lfloor\dfrac{t-20T_{\rm d}}{T_{\rm d}}\right\rfloor, & t>20T_{\rm d}.\end{cases} \tag{17}$$

Figure 6 shows the equilibria achieved by (15) with step-dwell excitation (17), and Figure 7 shows the zoomed-in open-loop response of q and u versus time. Note that q converges for each step.

Next, we consider adaptive quasi-static PI control of the single-backlash system with the step-dwell command

$$r(t)=\begin{cases}0.1\left\lfloor\dfrac{t}{T_{\rm d}}\right\rfloor, & t<10T_{\rm d},\\ 1-0.1\left\lfloor\dfrac{t-10T_{\rm d}}{T_{\rm d}}\right\rfloor, & t>10T_{\rm d},\end{cases} \tag{18}$$

with $T_{\rm d}=1000$ sec. The control $u(t)$ is updated with sample time $T_{\rm s}=2$ sec, that is, for $t\in\{k,k+T_{\rm s}\}$,

$$u(t)=v_k, \tag{19}$$

where v_k is given by (1) and

$$z_k=r(kT_{\rm s})-q(kT_{\rm s}). \tag{20}$$

Figure 8 shows the closed-loop response and the evolution of the adaptive PI gains. Finally, Figure 9 shows the input-output phase portrait of closed-loop response of the single-backlash system (15) under quasi-static control. The converged values of q are shown in large colored dots.

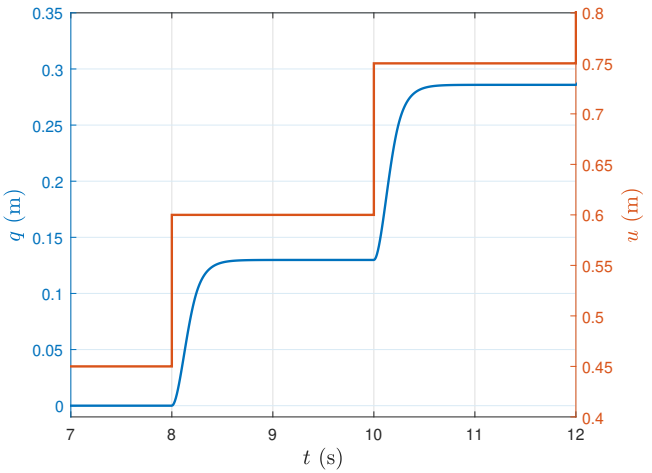

Fig. 7: Open-loop response of the single-backlash system (21)–(23) with the step-dwell excitation (18). Each step is applied with dwell time $T_{\rm d}$, and the state q converges for each step.

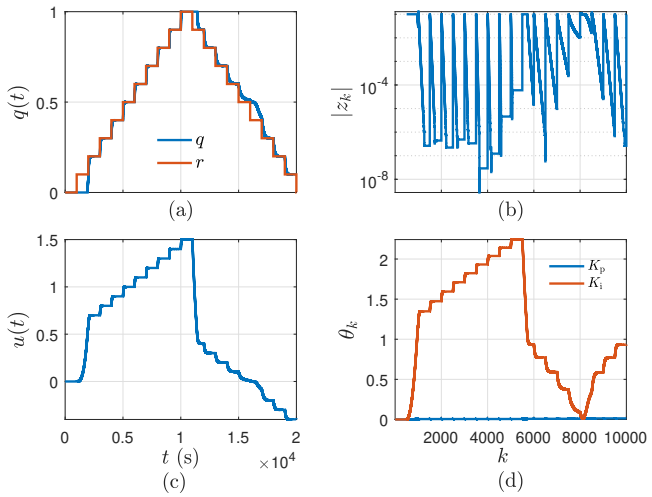

Fig. 8: Closed-loop response of the single-backlash system (15) with adaptive quasi-static PI control. (a) shows the state q, (b) shows the error variable z_k, (c) shows $u(t)$ given by the adaptive PI controller, and (d) shows the evolution of the PI gains $K_{\mathrm{p},k}$ and $K_{\mathrm{i},k}$.

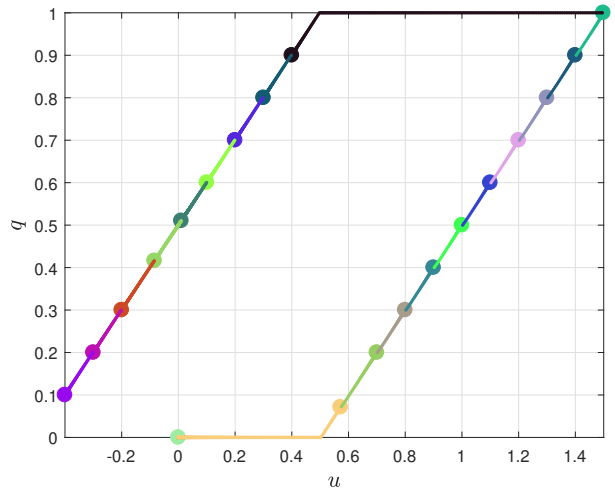

Fig. 9: Closed-loop response of the single-blacklash system (15) with the step-dwell command (18) using adaptive quasi-static PI control. The small colored dots indicate the sampled closed-loop response for each step, while the large dots in the corresponding color indicate the converged values of $q(t)$ and $u(t)$.

C. AQC of the Double-Backlash System

The equations of motion for the double-blacklash system shown in Figure 10 are given by

$$m_1\ddot{q}_1 + c_1\dot{q}_1 - k_1 d_{2w_1}(q_3 - q_1) = 0, \tag{21}$$

$$m_2\ddot{q}_2 + k_1 d_{2w_1}(q_3 - q_1) - k_2 d_{2w_2}(u - q_2) = 0, \tag{22}$$

$$c_2\dot{q}_3 - c_2\dot{q}_2 - k_1 d_{2w_1}(q_3 - q_1) = 0, \tag{23}$$

where d_{2w_1} and d_{2w_2} are given by (16). Let $m_1 = m_2 = 1$ kg, $c_1 = c_2 = 10$ N-s/m, $k_1 = k_2 = 100$ N/m, $w_1 = w_2 = 0.1$ m, $q_1(0) = q_2(0) = \dot{q}_1(0) = \dot{q}_2(0) = 0$, and let u be given by

$$u(t) = \begin{cases} 0.1\left\lfloor \dfrac{t}{T_{\mathrm{d}}} \right\rfloor, & t \le 10T_{\mathrm{d}}, \\ 1 - 0.1\left\lfloor \dfrac{t - 10T_{\mathrm{d}}}{T_{\mathrm{d}}} \right\rfloor, & t > 10T_{\mathrm{d}}, \end{cases} \tag{24}$$

where each step is applied with dwell time T_{d}. Figure 10 shows the equilibria achieved by (21)–(23) with the step-dwell excitation (24).

Next, we consider adaptive quasi-static PI control of the double-backlash system with the step-dwell command

$$r(t) = \begin{cases} 0.1\left\lfloor \dfrac{t}{T_{\mathrm{d}}} \right\rfloor, & t \le 10T_{\mathrm{d}}, \\ 1 - 0.1\left\lfloor \dfrac{t - 10T_{\mathrm{d}}}{T_{\mathrm{d}}} \right\rfloor, & t > 10T_{\mathrm{d}}, \end{cases} \tag{25}$$

with $T_{\mathrm{d}} = 1000$ sec. The control $u(t)$ is updated with sample time $T_{\mathrm{s}} = 2$ sec, that is, for $t \in \{k, k + T_{\mathrm{s}}\}$,

$$u(t) = v_k, \tag{26}$$

where v_k is given by (1) and

$$z_k = r(kT_{\mathrm{s}}) - q(kT_{\mathrm{s}}). \tag{27}$$

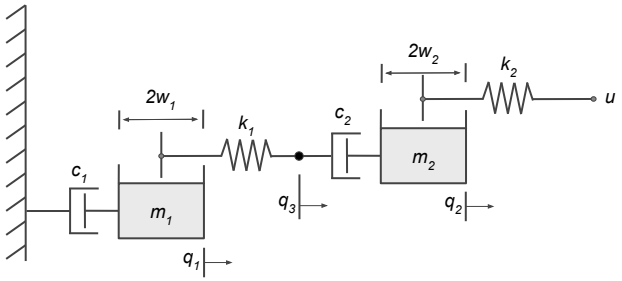

Fig. 10: Double-backlash system. The input u is the position of the right-hand endpoint of k_2, and the output q_1 is the position of the right-hand edge of m_1. The deadzone widths are $2w_1$ and $2w_2$.

IV. Conclusions

This paper applied adaptive digital PID control to quasi-static control of systems that are nonlinear, uncertain, and multistable. The approach was demonstrated on multistable systems involving unmodeled cubic and backlash nonlinearities having isolated equilibria or a continuum of equilibria. These examples suggest that adaptive digital PID control is a viable approach to quasi-static control of systems that are nonlinear, uncertain, and multistable. Future research will apply this technique to physical applications, such as aircraft flight control for trimmed flight and drag reduction, structural shape control, and process control.

References

[1] M. M. Seron, J. H. Braslavsky, and G. C. Goodwin, *Fundamental Limitations in Filtering and Control*. New York: Springer, 1997.

[2] J. C. Doyle, B. A. Francis, and A. R. Tannenbaum, *Feedback Control Theory*. Macmillan, 1992.

[3] J. B. Collings and D. J. Wollkind, "Metastability, hysteresis and outbreaks in a temperature-dependent model for a mite predator-prey interaction," *Math. Comp. Modelling*, vol. 13, pp. 91–103, 1990.

[4] D. Angeli and E. D. Sontag, "Multi-stability in monotone input/output systems," *Sys. Contr. Lett.*, vol. 51, pp. 185–202, 2004.

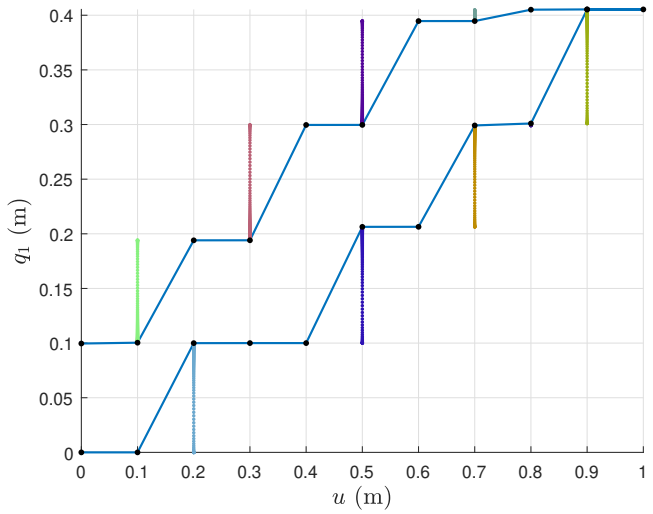

Fig. 11: Open-loop response of the double-backlash system (21)–(23) obtained with the step-dwell excitation (24). Each point on the blue curves corresponds to a Lyapunov- stable forced equilibrium and satisfies $d_{2w_1}(q_1 - u) = 0$. The colored vertical line segments show the trajectory of q_1 for each step. Note that q_1 may not change for every step since the step change in the input u is smaller than the total backlash width.

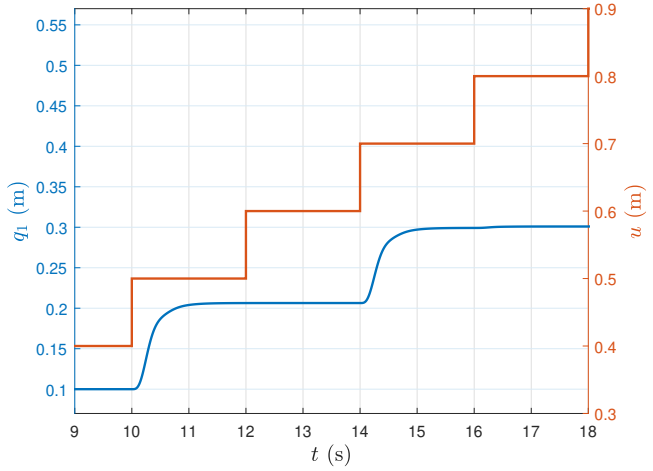

Fig. 12: Open-loop response of double-backlash system (21)–(23) with step-dwell excitation (24). The response settles in less than 2 sec, which is the sample time of the sampled-data controller. Note that q_1 may not change for every step since the step change in the input u is smaller than the total backlash width.

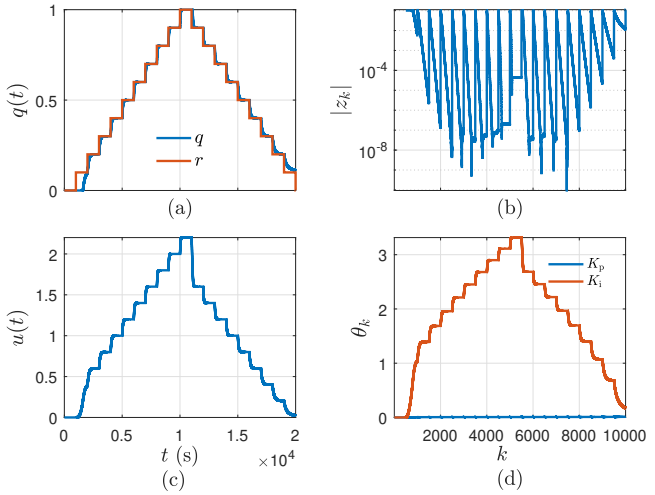

Fig. 13: Closed-loop response of the double-backlash system (21)–(23) with adaptive quasi-static PI control. (a) shows the state q_1, (b) shows the error variable z_k, (c) shows $u(t)$ given by the adaptive PI controller, and (d) shows the evolution of the gains $K_{\mathrm{p},k}$ and $K_{\mathrm{i},k}$.

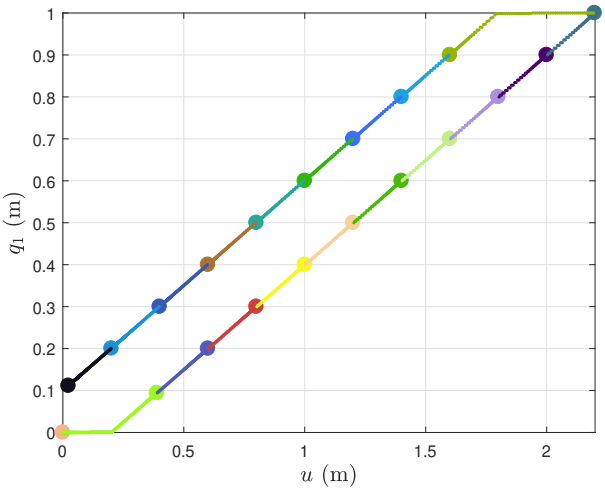

Fig. 14: Closed-loop response of the double-backlash system (21)–(23) under quasi-static PI control. The small colored dots indicate the sampled closed-loop response for each step, while the large dots in the corresponding color indicate the converged values of $q(t)$ and $u(t)$.

[5] D. Angeli, J. E. Ferrell, and E. D. Sontag, "Detection of multistability, bifurcations, and hysteresis in a large class of biological positive-feedback systems," *Proc. Natl. Acad. Sci.*, vol. 101, pp. 1822–1827, 2004.

[6] U. Feudel, "Complex dynamics in multistable systems," *Int. J. Bifurcation Chaos*, vol. 18, pp. 1607–1626, 2008.

[7] L. O. Chua and S. C. Bass, "A generalized hysteresis model," *IEEE Trans. Circuit Theory*, vol. 19, pp. 36–48, 1972.

[8] J. Oh and D. S. Bernstein, "Semilinear Duhem model for rate-independent and rate-dependent hysteresis," *IEEE Trans. Automat. Contr.*, vol. 50, pp. 631–645, 2005.

[9] D. S. Bernstein, "Ivory ghost," *IEEE Control Sys. Mag.*, vol. 27, pp. 16–17, 2007.

[10] M. Krasnoselski and A. Pokrovski, *Systems with Hysteresis*. Springer-Verlag, 1980.

[11] I. D. Mayergoyz, *Mathematical Models of Hysteresis*. Springer, 1991.

[12] J. W. Macki, P. Nistri, and P. Zecca, "Mathematical models for hysteresis," *SIAM Rev.*, vol. 35, pp. 94–123, 1993.

[13] A. Visintin, *Differential Models of Hysteresis*. Springer, 1994.

[14] M. Nordin and P. Gutman, "Controlling mechanical systems with backlash—a survey," *Automatica*, vol. 38, pp. 1633–1649, 2002.

[15] J. Oh, B. Drincic, and D. S. Bernstein, "Nonlinear Feedback Models of Hysteresis: Backlash, Bifurcation, and Multistability," *IEEE Control Sys. Mag.*, vol. 29, pp. 100–119, 2009.

[16] G. Tao and P. V. Kokotovic, *Adaptive Control of Systems with Actuator and Sensor Nonlinearities*. Wiley, 1996.

[17] A. N. Pisarchik and U. Feudel, "Control of multistability," *Physics Reports*, vol. 540, pp. 167–218, 2014.

[18] M. Kamaldar, S. A. U. Islam, S. Sanjeevini, A. Goel, J. B. Hoagg, and D. S. Bernstein, "Adaptive Digital PID Control of First-Order-Lag-Plus-Dead-Time Dynamics with Sensor, Actuator, and Feedback Nonlinearities," *Advanced Control for Applications*, vol. 1, pp. 1–46, 2019.